Journal of Applied Mechanics Vol.10, pp.839-846 (August 2007) JSCE

An Investigation on Lateral Intrusion Process of Water into Porous Media under Different Upstream Boundary Conditions

Bidur GHIMIRE*, Takashi HOSODA** and Shinichiro NAKASHIMA***

*Ph.D. Student, Department of Urban Management, Kyoto University (615-8540, Kyoto)
**Professor, Department of Urban Management, Kyoto University (615-8540, Kyoto)
***Research Associate, Pioneering Research Unit for Next Generation, Kyoto University (615-8540, Kyoto)

This paper deals with the lateral intrusion process of water into porous media consisting of large grain size, which seems to simulate the storm water storage into pervious road sub-base from a side drainage channel, under constant water level and constant inflow discharge conditions. The common fundamental equations for solid-liquid multiphase flows with the inertia term are used as the basic model. The fundamental characteristics of lateral intrusion process are firstly investigated theoretically using the depth averaged equations with the inertia term and the viscous or turbulent drag force terms in the momentum equation. It is pointed out that there are distinct two power law regions with respect to time in the unsteady intrusion processes. The theoretical results are verified by carrying out the vertical 2-D numerical simulation and simple hydraulic experiment.

Key words: *porous media, non-Darcy flow, similarity solution, pervious pavement, numerical simulation.*

1. Introduction

The flow of an incompressible fluid through a porous medium is a physical phenomenon of great importance in many practical situations. An important branch of porous media research involves the modeling of flow within the soil. The viscous, laminar incompressible flow with small porosity is represented by Darcy equation[1),2)]. The Darcy law assumes that the inertia force in the momentum equation is negligible compared with the other drag force and pressure terms.

In this paper, we deal with the lateral intrusion process into porous media consisting of large grain size, which seems to simulate the storm water storage into pervious road sub base from a side drainage channel, under constant water level and constant inflow discharge conditions. The common fundamental equations for solid-liquid multiphase flows with the inertia force term, which is neglected to simulate normal underground flows, are used as the basic model of this study because the pervious road sub-base material consists of large grain size material.

The fundamental characteristics of lateral intrusion process are firstly investigated theoretically using the depth averaged equations with the inertia term and the viscous or turbulent drag force terms in the momentum equation. Assuming the self-similarity distributions of depth and velocity, we derived the similarity solutions of intrusion process with the propagation of front position and the depth distribution under two boundary conditions. It is pointed out that there are distinct two power law regions with respect to in the intrusion processes.

The theoretical results derived in this study are verified by carrying out the numerical simulations and hydraulic experiments. The vertical 2-D numerical simulation is done applying the finite volume method with volume of fluid (VOF) technique. It is pointed out that the power law of propagation of front position, the distribution of depth, etc. can be reproduced in the results of simulations and hydraulic experiments.

2. Flow domain and boundary conditions of intrusion process

Two types of flow domains are considered for the study of intrusion dynamics of fluid into the porous media. Thus the flow fields are named as Case A for the domain subjected to constant upstream water level boundary and Case B for constant upstream discharge boundary condition. Fig. 1 and Fig. 2 show the schematic diagrams for two cases, respectively.

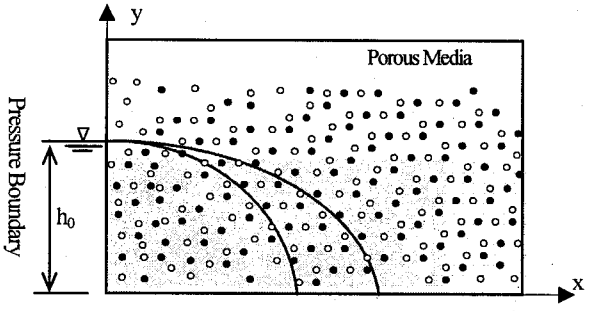

Fig. 1 Schematic diagram showing flow domain subjected to constant upstream water level boundary (Case A)

The speed of front propagation, the average velocity and the depth of free surface flow in the porous media have been studied and analyzed with the derivation of similarity solutions for each of the cases.

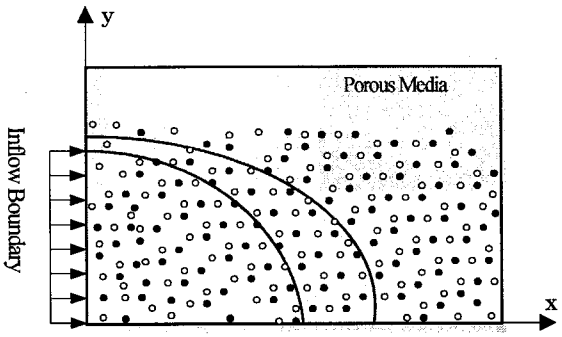

Fig. 2 Schematic diagram showing flow domain subjected to constant upstream inflow boundary (Case B)

3. Outline of the experimental setup

An experiment has been carried out for the evaluation of the proposed model. A transparent flume of 100mm width and 100mm height and length 750mm has been used. In the experiment 1mm glass beads were used as porous media and a constant water level of 85 mm was maintained at the left boundary as stated for Case A (Fig. 3 and Fig. 4). The experiment was carried out for the horizontal flume. The velocity and depth of flow with free surface have been taken using digital movie camera placed near the side of the flume. The position of front and depth of flow for different time is tracked by the image interpretation with the help of graduations made on the flume itself. The time dependence and the flow profile of the intrusion behaviour observed during the experiment were compared with the analytical solution and numerical simulation as well. The experimental conditions are given in the Table 1.

Table 1. Experimental Conditions

Parameters	Unit	Values
Water temperature	°C	14
Bed Slope	–	0
Size of glass bead (dia)	mm	1
Permeability (K)	m/s	0.01
Concentration of solid particles (C)	%	40
Flume dimensions (L, B, H)*	cm	75, 10, 10
Constant water level at u/s boundary, h_0	mm	85

* L: Length, B: Width and H: Height.

The experiment was carried out up to steady state. The permeability was also calculated using the hydraulic gradient when the system attained steady state. The measured steady state discharge and the flow depths have been used for the calculation of the value of permeability of the media.

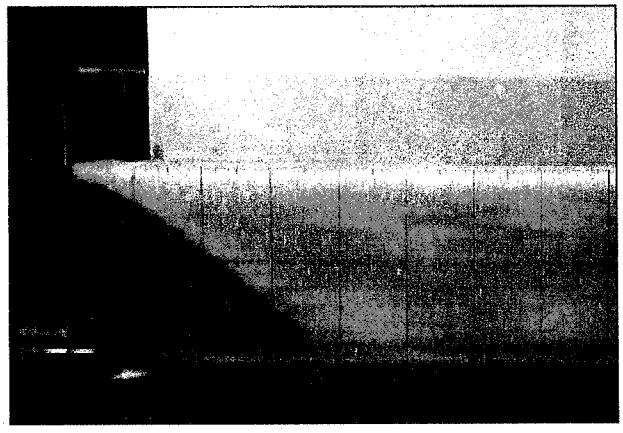

Fig. 3 Flow profile during the experiment (at time 5 sec)

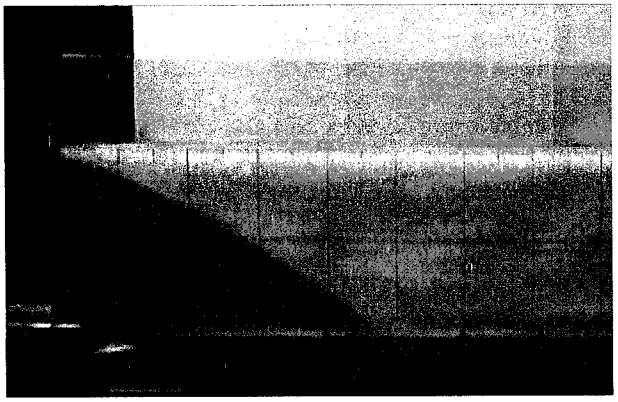

Fig. 4 Flow profile during the experiment (at time 10 sec)

4. Theoretical considerations

The continuity and momentum equations for solid-liquid multiphase flow given in the section 5 are considered as the basic equations. In order to investigate fundamental characteristics of intrusion process, the simplified depth averaged equations with the inertia term are used integrating the basic equations from the bottom to the surface under the assumption of hydrostatic pressure distribution. The analytical similarity solutions are derived for different possible flow regions in this section.

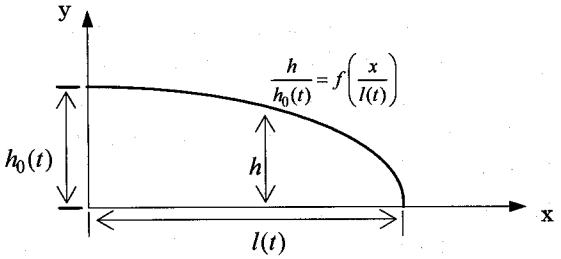

Fig. 5 Definition of similarity distribution of flow depth

The approximate solutions of depth and velocity distributions are derived based on the similarity of depth averaged flow to clarify the fundamental characteristics of lateral intrusion of water under two boundary conditions. The method based on similarity was applied to

the dam break flow of viscous fluid where temporal and spatial distribution of depth, velocity and front position were derived analytically balancing the pressure gradient and viscous terms[3),4)]. The method assumes the similarity of the distribution using characteristics depth and length as shown in Fig. 5. In this paper we derive the similarity solutions of two regions using the similar method where Inertia-Pressure terms and Pressure-Drag terms are balanced under two different boundary conditions.

4.1 Basic equations

The basic equations for continuity and momentum for one dimensional depth averaged flow with the inertia term and the drag resistance term can be written as:

$$\frac{\partial\{(1-C)h\}}{\partial t}+\frac{\partial\{(1-C)hU\}}{\partial x}=0 \tag{1}$$

$$\frac{\partial\{(1-C)hU\}}{\partial t}+\frac{\partial\{(1-C)hU^2\}}{\partial x}=-(1-C)gh\frac{\partial z_s}{\partial x}+\frac{\partial}{\partial x}\left\{(1-C)\frac{\tau_{xx}}{\rho}h\right\}-\frac{\tau_{bx}}{\rho}-\frac{R_x}{\rho}h \tag{2}$$

where t is time, x is spatial coordinate, h is the flow depth, U is the depth averaged velocity, z_s is the free surface elevation, τ_{xx} is the viscous stress, τ_{bx} is the bottom shear stress and ρ is the density of water. For the analytical study, the volumetric concentration of solid particles C is taken constant. The last term with R_x of equation (2) represents the Darcy's resistance term. Hence for the conventional flow in porous media if we neglect the shear stress and inertia terms, as is valid for Darcy's theory, in equation (2), we get the expression of the Darcy's Law in which the term R_x is defined as

$$\frac{R_x}{\rho}=(1-C)g\frac{(1-C)}{K}U \tag{3}$$

where K is permeability of the porous medium. The resistance law of turbulent flow is also considered later. Taking (1-C) and K to be constant and neglecting the shear stress terms in equations (1) and (2) we get the following set of continuity and momentum equation for the analytical study subjected to various boundary conditions.

$$\frac{\partial h}{\partial t}+\frac{\partial hU}{\partial x}=0 \tag{4}$$

$$\frac{\partial U}{\partial t}+U\frac{\partial U}{\partial x}+g\frac{\partial h}{\partial x}=-C_X U \tag{5}$$

where C_X is defined as $C_X=\dfrac{g(1-C)}{K}$.

Two types of boundary conditions subjected to the flow domain are Pressure boundary (Case A) and Discharge boundary (Case B) which will be discussed in the subsequent sections.

4.2 Solutions for similarity of distribution

The analytical solutions based on similarity of distributions have been derived for both the cases stated earlier. The definition of the similarity distributions of the depth and velocity are firstly defined using characteristic depth, length and velocity.

(1) Constant water level condition (Case A)

For the solution using similarity distribution, let us define flow depth and velocity as:

$$h=h_0F\left(\frac{x}{l(t)}\right),\quad U=U_0G\left(\frac{x}{l(t)}\right) \tag{6}$$

where h_0 is constant water level at the upstream end of flow domain, U_0 the velocity at upstream end and $x/l(t)=\xi$. The functions F and G are the distribution functions for depth and velocity. Then from equations (4) and (5) we get

$$-\xi\frac{dF}{d\xi}\frac{dl}{dt}+U_0G\frac{dF}{d\xi}+U_0F\frac{dG}{d\xi}=0 \tag{7}$$

$$G\frac{dU_0}{dt}-\frac{U_0}{l}\xi\frac{dG}{d\xi}\frac{dl}{dt}+\frac{U_0^2}{l}G\frac{dG}{d\xi}+g\frac{h_0}{l}\frac{dF}{d\xi}=-C_xU_0G \tag{8}$$

Introducing the characteristic time, length and velocity as

$$T_0=\left(\frac{h_0}{g}\right)^{\frac{1}{2}},\quad L_0=h_0\ \text{ and }\ V_0=(gh_0)^{\frac{1}{2}} \tag{9}$$

It will be shown that the power laws with respect to time given by equation (10) are valid for the dominance of the combination of two terms of Inertia-Pressure and Pressure-Drag regions.

$$U_0=\alpha V_0(t')^a,\quad h_0=\beta L_0(t')^b\ \text{ and }\ l=\gamma L_0(t')^c \tag{10}$$

where α, β and γ are constants and t' is the non dimensional time defined as $t'=t/T_0$. Using equations (9) and (10) equations (7) and (8) reduce to (11) and (12) as below,

$$-\xi\frac{\gamma L_0}{T_0}ct'^{c-1}\frac{dF}{d\xi}+\alpha V_0t'^a\frac{dGF}{d\xi}=0 \tag{11}$$

$$\underbrace{\alpha\frac{V_0}{T_0}at'^{a-1}G-\alpha\frac{V_0}{T_0}ct'^{a-1}\xi\frac{dG}{d\xi}}_{inertia(unsteady)}+\underbrace{\frac{\alpha^2}{\gamma}\frac{V_0^2}{L_0}t'^{2a-c}G\frac{dG}{d\xi}}_{inertia(convection)}+\underbrace{\frac{\beta}{\gamma}gt'^{b-c}\frac{dF}{d\xi}}_{pressure}=\underbrace{-C_x\alpha V_0t'^aG}_{drag} \tag{12}$$

Due to the constant water level boundary condition h_0 is constant i.e.

$$b = 0 \tag{13}$$

From equation (11) we can write

$$c - a = 1 \tag{14}$$

For the determination of the values of power coefficients a, b and c each combination of equation (12) such as Inertia-Pressure terms and Pressure-Drag terms are taken and solved for the coefficients. The results are given below.

(i) Inertia-Pressure region:

$$a = 0,\ b = 0 \ \text{ and } \ c = 1 \tag{15}$$

(ii) Pressure-Drag region:

$$a = -\frac{1}{2},\ b = 0 \ \text{ and } \ c = \frac{1}{2} \tag{16}$$

(iii) Inertia-Drag region:

No solution is obtained for this region.

The similarity solution for the derived powers has been sought for different regions as depicted by the transformed continuity and momentum equations for the above two possible regions as given below.

(i) Inertia-Pressure region

The sets of equations for this region will then be given by

$$-\frac{\gamma L_0}{T_0}\xi\frac{dF}{d\xi} + \alpha V_0\frac{dGF}{d\xi} = 0 \tag{17}$$

$$-\alpha\frac{V_0}{T_0}\xi\frac{dG}{d\xi} + \frac{\alpha^2}{\gamma}\frac{V_0^2}{L_0}G\frac{dG}{d\xi} + \frac{\beta}{\gamma}g\frac{dF}{d\xi} = 0 \tag{18}$$

Also the velocity of front U_F can be written as

$$U \text{ at } x = l(t) \ \text{ i.e. } \ U_F = \frac{dl}{dt} = \gamma L_0 c t'^{c-1}\frac{1}{T_0} = \frac{\gamma L_0}{T_0} \tag{19}$$

U at $x = 0$ is given by $U_0 = \alpha V_0$. Assuming G and F as the function of ξ as below,

$G = 1\text{-}A\xi$, A = const.

$F = 1\text{-}\xi$

Using the values of G and F in equations (17) and (18) and after some simplification we get,

$$\alpha V_0 = \sqrt{gh_0},\ \beta L_0 = h_0 \ \text{ and } \ \gamma L_0 = 2T_0\sqrt{gh_0} \tag{20}$$

The front position $l(t)$ and the velocity of front U_F is derived as

$$l = \gamma L_0\left(\frac{t}{T_0}\right)^c = 2\sqrt{(gh_0)}\ \ t \tag{21}$$

$$U_F = \frac{dl}{dt} = \gamma L_0 c\left(\frac{t}{T_0}\right)^{c-1}\frac{1}{T_0} = 2\sqrt{gh_0} \tag{22}$$

The flow depth and velocity is then derived as

$$h = h_0 F\left(\frac{x}{l(t)}\right) = h_0\left(1 - \frac{x}{l(t)}\right) = h_0\left(1 - \frac{x}{2\sqrt{gh_0}}\frac{1}{t}\right) \tag{23}$$

$$U = U_0 G\left(\frac{x}{l(t)}\right) = \left(\sqrt{gh_0}\right)\left(1 + \frac{x}{l(t)}\right) \tag{24}$$

(ii) Pressure-Drag region

The governing equations for this region can be written as

$$-\frac{\gamma L_0}{2T_0}\xi\frac{dF}{d\xi} + \alpha V_0\frac{dGF}{d\xi} = 0 \tag{25}$$

$$\frac{\beta}{\gamma}g\frac{dF}{d\xi} = -C_x\alpha V_0 G \tag{26}$$

Thus equations (25) and (26) yield

$$\alpha V_0 = \frac{1}{2}\left(\frac{gh_0}{T_0 C_x}\right)^{\frac{1}{2}},\ \beta L_0 = h_0 \ \text{ and}$$

$$\gamma L_0 = \left(\frac{4gT_0 h_0}{C_x}\right)^{\frac{1}{2}} \tag{27}$$

Now the front position $l(t)$ and front velocity U_F is derived as

$$l = \left(\frac{4gh_0}{C_x}\right)^{\frac{1}{2}} t^{\frac{1}{2}} \ \text{ and } \ U_F = \frac{dl}{dt} = \left(\frac{gh_0}{C_x}\right)^{\frac{1}{2}} t^{-\frac{1}{2}} \tag{28}$$

Similarly the flow depth and velocities can be written as

$$h = h_0\left(1 - \frac{x}{l(t)}\right) \text{ and } U = \frac{1}{2}\left(\frac{gh_0}{C_x}\right)^{\frac{1}{2}}\left(1 + \frac{x}{l(t)}\right)t^{-\frac{1}{2}} \tag{29}$$

(2) Constant discharge condition (Case B)

For the solution using similarity law, the flow depth and velocity have been defined as

$$h = h_0 F\left(\frac{x}{l(t)}\right),\quad U = U_0 G\left(\frac{x}{l(t)}\right) \tag{30}$$

where h_0 and U_0 are the inflow depth and velocity respectively and the constant discharge condition is given by the relation $h_0U_0 = q_0$ (constant). Using these relations, equations (4) and (5) are reduced to equations (31) and (32) as

$$\frac{dh_0}{dt}F - \frac{h_0}{l}\xi\frac{dF}{d\xi}\frac{dl}{dt} + q_0\frac{1}{l}G\frac{dF}{d\xi} + q_0\frac{1}{l}F\frac{dG}{d\xi} = 0 \tag{31}$$

$$\frac{dU_0}{dt}G - \frac{U_0}{l}\xi\frac{dG}{d\xi}\frac{dl}{dt} + \frac{U_0^2}{l}G\frac{dG}{d\xi} + g\frac{h_0}{l}\frac{dF}{d\xi} = -C_x U_0 G \tag{32}$$

Introducing the characteristic time T_0, length L_0 and velocity V_0 as

$$T_0 = \left(\frac{q_0}{g^2}\right)^{\frac{1}{3}},\quad L_0 = \left(\frac{q_0^2}{g}\right)^{\frac{1}{3}} \text{ and } V_0 = (gq_0)^{\frac{1}{3}} \tag{33}$$

And defining U_0, h_0 and l as

$$U_0 = \alpha V_0\left(\frac{t}{T_0}\right)^a,\quad h_0 = \beta L_0\left(\frac{t}{T_0}\right)^b \text{ and } l = \gamma L_0\left(\frac{t}{T_0}\right)^c \tag{34}$$

where α, β and γ are constants, we will derive a power relation as given in the subsequent section. Now substituting equation (34) in (7) and (8), following two equations are derived,

$$\beta\frac{L_0}{T_0}bt'^{b-1}F - \beta\frac{L_0}{T_0}ct'^{b-1}\xi\frac{dF}{d\xi} + \frac{q_0}{\gamma L_0}t'^{-c}\frac{dGF}{d\xi} = 0 \tag{35}$$

$$\underbrace{\alpha\frac{V_0}{T_0}at'^{a-1}G - \alpha\frac{V_0}{T_0}ct'^{a-1}\xi\frac{dG}{d\xi}}_{inertia(unsteady)} + \underbrace{\frac{\alpha^2}{\gamma}\frac{V_0^2}{L_0}t'^{2a-c}G\frac{dG}{d\xi}}_{inertia(convection)} + \underbrace{\frac{\beta}{\gamma}gt'^{b-c}\frac{dF}{d\xi}}_{pressure} = \underbrace{-C_x\alpha V_0 t'^a G}_{drag} \tag{36}$$

The constant discharge condition is given by

$$\alpha\beta V_0 L_0 (t')^{a+b} = q_0 (= const.) \tag{37}$$

This condition gives

$$a + b = 0 \tag{38}$$

The transformed continuity equation (35) gives

$$b + c = 1 \tag{39}$$

For the determination of the values of power coefficients a, b and c each combination of equation (36) is taken and solved for the coefficients. The results are shown below.

(i) Inertia-Pressure region:

$$a = 0,\quad b = 0 \text{ and } c = 1 \tag{40}$$

(ii) Pressure-Drag region:

$$a = -\frac{1}{3},\quad b = \frac{1}{3} \text{ and } c = \frac{2}{3} \tag{41}$$

(iii) Inertia-Drag region:

No solution is obtained for this region.

The values of the power coefficients as derived analytically and as obtained numerically clearly shows the two regions: Inertia-Pressure region and Pressure-Drag region. The similarity solution for the derived powers has been sought for different regions as depicted by the transformed continuity and momentum equation as given below.

(i) Inertia-Pressure region

For this region the sets of equations (35) and (36) reduce to equations (42) and (43) as

$$-\beta\frac{L_0}{T_0}\xi\frac{dF}{d\xi} + \frac{q_0}{\gamma L_0}\frac{dGF}{d\xi} = 0 \tag{42}$$

$$-\alpha\frac{V_0}{T_0}\xi\frac{dG}{d\xi} + \frac{\alpha^2}{\gamma}\frac{V_0^2}{L_0}G\frac{dG}{d\xi} + \frac{\beta}{\gamma}g\frac{dF}{d\xi} = 0 \tag{43}$$

Using the same formulation applied to the constant water level case, the similarity solutions of the flow depth and velocity are given by

$$h = h_0 F\left(\frac{x}{l(t)}\right) = \left(\frac{q_0^2}{g}\right)^{\frac{1}{3}}\left(1 - \frac{x}{l(t)}\right) \tag{44}$$

$$U = U_0 G\left(\frac{x}{l(t)}\right) = (gq_0)^{\frac{1}{3}}\left(1 + \frac{x}{l(t)}\right) \tag{45}$$

where U_0, h_0 and $l(t)$ are defined as follows.

$$U_0 = (gq_0)^{\frac{1}{3}},\quad h_0 = \left(\frac{q_0^2}{g}\right)^{\frac{1}{3}} \text{ and } l(t) = 2(gq_0)^{\frac{1}{3}}t \tag{46}$$

(iii) Pressure-Drag region

For this region the sets of equations (35) and (36) reduces to (47) and (48) as:

$$\frac{\beta L_0}{T_0}\frac{1}{3}F - \frac{\beta L_0}{T_0}\frac{2}{3}\xi\frac{dF}{d\xi} + \frac{q_0}{\gamma L_0}\frac{dGF}{d\xi} = 0 \tag{47}$$

$$\frac{\beta}{\gamma}g\frac{dF}{d\xi} = -C_x\alpha V_0 G \tag{48}$$

Using the same formulations defined earlier the solution for flow depth and velocity for Pressure-Drag (PD) region is given as follows,

$$h = h_0 F\left(\frac{x}{l(t)}\right) = \left(\frac{2q_0^2 C_x}{g}\right)^{\frac{1}{3}} t^{\frac{1}{3}}\left(1 - \frac{x}{l(t)}\right) \tag{49}$$

$$U = U_0 G\left(\frac{x}{l(t)}\right) = \left(\frac{q_0 g}{2C_x}\right)^{\frac{1}{3}}\left(1 + \frac{1}{3}\frac{x}{l(t)}\right)t^{-\frac{1}{3}} \tag{50}$$

where U_0, h_0 and l are derived as:

$$U_0 = \left(\frac{q_0 g}{2C_x}\right)^{\frac{1}{3}} t^{-\frac{1}{3}},\quad h_0 = \left(\frac{2q_0^2 C_x}{g}\right)^{\frac{1}{3}} t^{\frac{1}{3}} \text{ and}$$

$$l = 2\left(\frac{q_0 g}{2C_x}\right)^{\frac{1}{3}} t^{\frac{2}{3}} \tag{51}$$

4.3 Solutions for similarity of distribution for turbulent flow

Theoretical derivation for the turbulent flow in porous media composed of large grains is made here. The momentum sink term contributing to the pressure gradient due to porous media is assumed to be proportional to the fluid velocity squared. Hence the resistance term can be written as

$$\frac{R_x}{\rho} = C_T U^2 \tag{52}$$

The governing equations for this case can be written as

$$\frac{\partial h}{\partial t} + \frac{\partial hU}{\partial x} = 0 \tag{53}$$

$$\frac{\partial U}{\partial t} + U\frac{\partial U}{\partial x} + g\frac{\partial h}{\partial x} = -C_T U^2 \tag{54}$$

where C_T is the coefficient used for the resistance law of turbulent flow. In this study, we did not consider the effect of Reynold's number on C_T so that the coefficient C_T is assumed to be dependent only on the porous media characteristics. The right hand side term of equation (54) is important where Darcy law is not applicable due to high flow velocities[5]. The similar analysis has also been made for turbulent flows in the porous media having large permeability. The theoretical results obtained for different boundary conditions of flow are given below.

(1) Constant water level condition

The powers a, b and c are the temporal powers of the velocity, depth of flow at the origin and front position respectively as defined in the preceding section for Case A. The values were derived in the same way as it was done in section 4.2 and are presented below

(i) Inertia-Pressure region:

$$a = 0,\ b = 0 \ \text{ and } \ c = 1 \tag{55}$$

(ii) Pressure-Drag region:

$$a = -\frac{1}{3},\ b = 0 \ \text{ and } \ c = \frac{2}{3} \tag{56}$$

(2) Constant discharge condition

The powers a, b and c are the temporal powers of the velocity, depth of flow at the origin and front position respectively as defined in the previous section for Case B. The values are derived here in the same way as it has been done in preceding section. Only the results are presented below,

(i) Inertia-Pressure region:

$$a = 0,\ b = 0 \ \text{ and } \ c = 1 \tag{57}$$

(ii) Pressure-Drag region:

$$a = -\frac{1}{4},\ b = \frac{1}{4} \ \text{ and } \ c = \frac{3}{4} \tag{58}$$

The theoretical derivation thus shows two possible flow regions: Inertia-Pressure and Pressure-Drag region.

5. Numerical simulation

5.1 Basic equations

The governing equations in vertical two-dimension for the flow in porous and/or free region in the composite form are formulated below for the incompressible fluid. The equation for the phase continuity of the fluid is given by

$$\frac{\partial(1-C)}{\partial t} + \frac{\partial(1-C)u}{\partial x} + \frac{\partial(1-C)v}{\partial y} = 0 \tag{59}$$

and the momentum equations with the Darcy-term can be written as

$$\begin{aligned}&\frac{\partial\{(1-C)u\}}{\partial t} + \frac{\partial\{(1-C)u^2\}}{\partial x} + \frac{\partial\{(1-C)uv\}}{\partial y} \\ &= -(1-C)\frac{1}{\rho}\frac{\partial p}{\partial x} + \nu\left(\frac{\partial^2(1-C)u}{\partial x^2} + \frac{\partial^2(1-C)u}{\partial y^2}\right) - \frac{R_x}{\rho} + (1-C)g_x\end{aligned} \tag{60}$$

and,

$$\begin{aligned}&\frac{\partial\{(1-C)v\}}{\partial t} + \frac{\partial\{(1-C)uv\}}{\partial x} + \frac{\partial\{(1-C)v^2\}}{\partial y} \\ &= -(1-C)\frac{1}{\rho}\frac{\partial p}{\partial y} + \nu\left(\frac{\partial^2(1-C)v}{\partial x^2} + \frac{\partial^2(1-C)v}{\partial y^2}\right) - \frac{R_y}{\rho} + (1-C)g_y\end{aligned} \tag{61}$$

where, $R_x = \rho\frac{g(1-C)^2}{K}u$ and $R_y = \rho\frac{g(1-C)^2}{K}v$.

In above equations u and v are the velocity components of fluid in x and z directions respectively; ρ is fluid density and ν the kinematic viscosity. K and C are the hydraulic conductivity and solid phase concentration of the media so the term (1- C) represents the porosity of the media. The Darcy's velocity and the pore space velocity are related as

$$\mathbf{U} = (1-C)\mathbf{V} \tag{62}$$

where, $\mathbf{U}$ is Darcy's velocity or Darcy's flux and $\mathbf{V}$ is the pore velocity vector (u,v). The hydraulic conductivity for laminar flow in porous media can be found by Kozeny-Carman formula in which K is given by

$$K = \frac{\varepsilon^3 d^2}{180(1-\varepsilon)^2}\frac{g}{\nu} \tag{63}$$

where ε and d are the porosity and particle diameter respectively.

A number of numerical runs have been made for different values of hydraulic parameters and the boundary conditions as well which are listed in Table 2.

Table 2. List of Numerical Run

Numerical Run	Case	Parameters
RUN1	A	K=0.250m/s, C=0.6, h_0=0.050m
RUN2	A	K=0.010m/s, C=0.6, h_0=0.085m
RUN3	B	K=0.005m/s, C=0.5, U_0=0.01m/s
RUN4	B	K=0.010m/s, C=0.6, U_0=0.05m/s

5.2 Numerical methods

The equations (59) to (61) are solved by finite volume method in a staggered computational grid where velocities are defined at the cell faces and all the scalar variables are defined at the cell centre. The pressure is iteratively adjusted using Highly Simplified Marker and Cell (HSMAC) method[6]. The velocity changes induced by each pressure change are added to the velocities computed before, enforcing thereby to satisfy the continuity equation.

The free surface kinematics is traced using VOF technique both in porous and free flow conditions[7]. For the porous flow domain the time evolution of the fraction of fluid function (1- *C*)*F* is governed by the following relation

$$\frac{\partial(1-C)F}{\partial t}+\frac{\partial u(1-C)F}{\partial x}+\frac{\partial v(1-C)F}{\partial y}=0 \qquad (64)$$

where (1- *C*)*F* represents the portion of cell occupied by the fluid i.e. cell saturation[8]. The model is applied for the porous media subjected to two different flow boundary conditions as stated in the previous section.

6. Results and discussions

The theoretical results given in the previous sections have been verified using the results of simulations.

The sample of velocity profiles obtained for the numerical experiments are shown in Fig. 6. This result of numerical simulation for Case B shows that there is increase in depth near the upstream boundary ($x = 0$) in the Pressure-Drag region as depicted by the equation (41) with temporal power b = 1/3 for the case considered.

Fig. 7 and Fig. 8 show the position of front verses time for Case A and Case B, respectively. These results of the numerical runs presented here clearly show the two regions of Inertia-Pressure and Pressure-Drag for both cases. The discrepancy in the Fig.7 (Case A) for Inertia-Pressure region shows that it takes sometime to realize self-similarity distribution of depth and velocity, but the temporal power of 1.0 is still valid. The results for case B (Fig. 8) are in close agreement with the analytical solution derived with similarity assumption.

The value of permeability for the numerical simulation of the experiment has been calculated from the equation (63) and it was compared with the values obtained from both the experiment and analytical solution. The results are shown in Table 3.

Table 3. Comparison of Permeabilities

Methods	Permeability (m/s)	Remarks
Kozeny-Carman formula	0.010	Equation (63)
Hydraulic grade line	0.010	From experiment
Analytical (PD) formula	0.009	Equation (28)

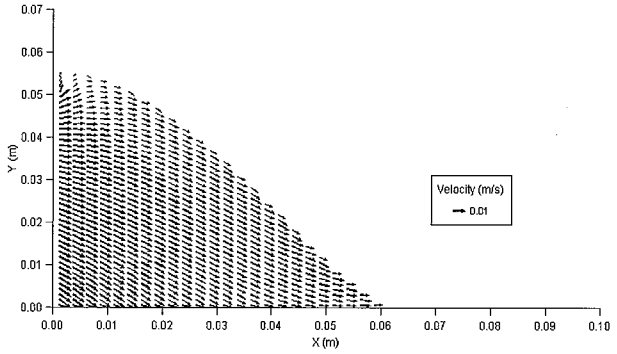

Fig. 6 (a)

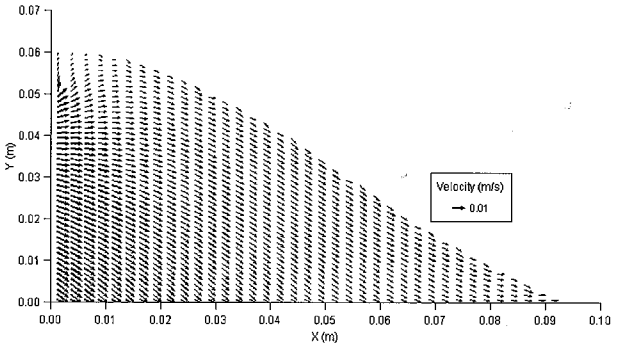

Fig. 6 (b)

Fig. 6 Velocity Profiles for Case B (RUN3) for (a) time 5s and (b) time 10s

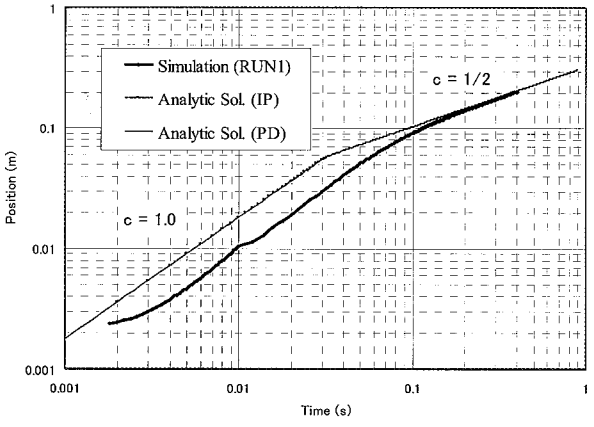

Fig .7 Temporal position of front under constant upstream water level (Case A)

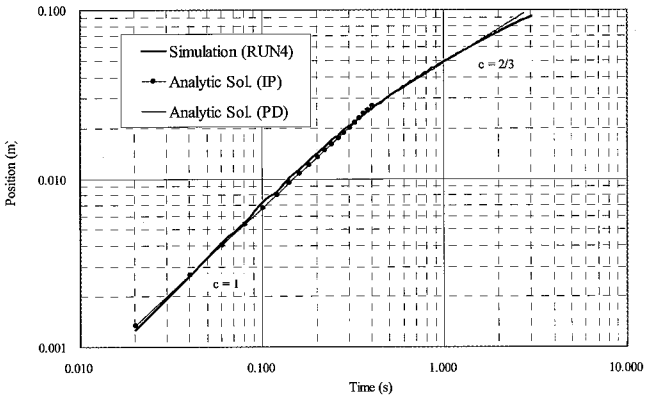

Fig.8 Temporal position of front under constant discharge (Case B)

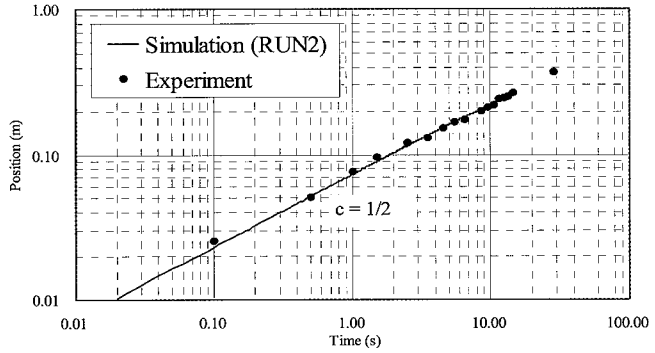

Fig.9 Temporal position of front under constant upstream water level (Case A)

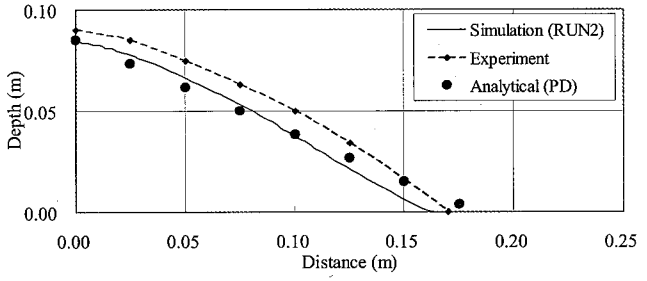

Fig. 10 (a)

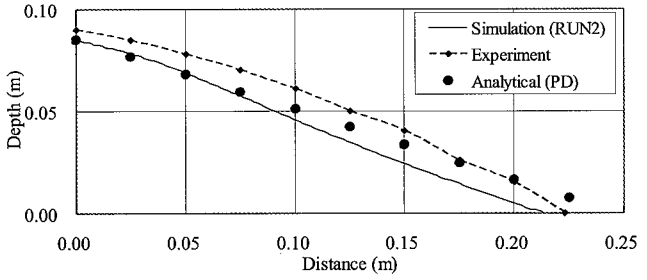

Fig. 10 (b)

Fig.10 Flow Profiles for constant upstream water level for (a) time 5s and (b) time 10s

Fig.9 shows the comparison between the experiment and the simulation. Since the velocity of front obeys temporal power of 1/2 we can point out the dominance of the Pressure-Drag region for low permeable media. The flow profiles are reproduced in the numerical run which is in close agreement with that of the experiment (Fig. 10). The experimental depths are slightly greater than that of the analytical and numerically simulated values. The reason may be due to the continuous rise of capillary fringe which was also observed in the experiment.

7. Conclusions

In this paper, the lateral intrusion processes of water into porous media under two boundary conditions are studied using the non-Darcy equation with the inertia term in the equation of motion. The results are summarized as follows:

(1) If we assume similarity distributions of depth and velocity and the dominance of the two terms of inertia-pressure and pressure-drag, the temporal power solutions for characteristic depth, length and velocity can be derived for inertia-pressure(IP) region and pressure-drag(PD) region respectively under two boundary conditions. The similarity distributions are also derived analytically.

(2) The vertical 2-D numerical simulations of flows were carried out using VOF method. The numerical results showed that IP region appeared first with the temporal power derived theoretically and PD region followed IP region.

(3) PD region was observed in the hydraulic experiment with glass beads of diameter 1mm. The spatial profile of depth of simulation is in good agreement with the experiments.

This research will be continued to make clear the region of the non-dimensional parameter where non-Darcy effect should be taken into account. The existence of IP region will be verified by the experiment with large size glass beads.

References

1) Beavers, G. S. and Joseph, D. D., Boundary conditions at the natural permeable wall, *J. Fluid Mech.*, 30, 197–207, 1967.
2) Hanspal, N.S., Waghode, A. N., Nassehi, V. and Wakeman, R., Numerical Analysis of coupled Stokes/Darcy Flows in Industrial Filtrations, Transport in Porous Media, Springer, 64, 73–101, 2006.
3) Herbert, E. H., The propagation of two-dimensional and axisymmetric viscous gravity currents over a rigid horizontal surface, *J. Fluid Mech.*, 121, 43–58, 1982.
4) Hosoda, T., Kokado, T. and Miyagawa, T., Flow characteristics of viscous fluids on the basis of self-similarity law and its applications to high flow concrete., *J. of Applied Mech., JSCE,* 3, 313-321, 2000.
5) Harry, R. C., Seepage, Drainage, and flow nets, John Wiley & Sons, Newyork, 1989.
6) Hirt, C.W. and Cook, J.L., Calculating Three Dimensional Flows around structures and over Rough Terrain, *J. Comput. Phys.*, 10, 324-340, 1972.
7) Hirt, C.W. and Nichols, B.D., Volume of fluid (VOF) method for the dynamics of free boundaries, *J. Comput. Phys.*, 39, 201-225, 1981.
8) Jacimovic, N., Hosoda, T., Kishida, K. and Ivetic, M., Numerical Solution of the Navier-Stokes equations for incompressible flow in porous media with free surface boundary, *J. of Applied Mech., JSCE,* 8, 225-231, 2005.

(Received : April 12, 2007)